11th World Congress on Computational Mechanics (WCCM XI)
5th European Conference on Computational Mechanics (ECCM V)
6th European Conference on Computational Fluid Dynamics (ECFD VI)
E. Oñate, J. Oliver and A. Huerta (Eds)

# CHANG-HSIEH-CHEN LOW-REYNOLDS *k-ε* TURBULENCE MODEL *ADAPTATION TO STUDY THE FLOW OF CONCENTRATED PULP SUSPENSIONS IN PIPES*

**C. COTAS[†], F. GARCIA[†], P. FERREIRA[†], P. FAIA[††], D. ASENDRYCH[†††] AND M.G. RASTEIRO[†*]**

[†] Chemical Process Engineering and Forest Products Research Centre (CIEPQPF)
Chemical Engineering Department of FCTUC
Rua Sílvio Lima, Pólo II, 3030-790 Coimbra, Portugal
[*] e-mail: mgr@eq.uc.pt, www.uc.pt/fctuc/deq/ciepqpf

[††] Electrical and Computers Engineering Department, University of Coimbra, Portugal

[†††] Faculty of Mechanical Engineering and Computer Science, Częstochowa University of Technology, Poland

**Key Words:** *non-Newtonian fluid, Chang-Hsieh-Chen turbulence model, damping function, drag reduction.*

**Abstract.** Computational Fluid Dynamics (CFD) tools can be applied successfully to predict the turbulent pipe flow of pulp suspensions. This strategy allows to avoid the design of industrial equipment based on empirical correlations. The present work investigated the turbulent pipe flow of concentrated *Eucalyptus* pulp suspensions. The numerical study was performed using the ANSYS FLUENT® CFD software [ANSYS FLUENT® 13.0.0, ANSYS FLUENT Inc., 2010]. A pseudo-homogeneous approach was applied in this work. The non-Newtonian behavior of the pulp suspensions was introduced into the CFD code by considering the pulp viscosity as a function of a local shear rate. Additionally, the model took into account a presence of a water annulus at the pipe wall surrounding the flow core. The Chang-Hsieh-Chen [1,2] low-Re *k-ε* turbulence model was selected in this study as the one allowing to account for a *drag reduction* effect in the pulp suspension flow as already shown in the previous work of the authors [3]. Moreover, as referred in [2] the CHC turbulence model is more universal than the other low-Re models since its constants are the same as those conventionally used for the standard *k-ε* model. The applicability of the CHC model to reproduce the drag reduction effect has been tested with a damping function adopted from the work of Malin [4] who studied the pipe flow of a power-law fluid. In order to better fit the available reference experimental data the damping function proposed in [4] has been modified by varying its parameters. A good correspondence between the velocity profiles reported in literature [5] and those obtained numerically was achieved. As the key indicator of the model appropriateness the pressure drop values obtained experimentally were used.

## 1 INTRODUCTION

The knowledge of the flow behavior of concentrated pulp suspensions has a great importance in the pulp and paper industry since the pulp's flow influences the characteristics of the pulp in pipes which affects the properties of the final product. The optimum design and process operation, which leads to higher production and process efficiency, lower costs and improved product quality, are nowadays the key issues of the pulp and paper industry. In this kind of industry, low energy efficiency and high process costs are mainly due to an incorrect design of the pump and flow systems in the different stages of the process. Despite of the growing interest on the experimental and numerical studies of pulp suspensions flow, which remains poor and incomplete, the design of the most process equipment is still based on empirical correlations. Computational tools, such as, for example CFD tools, can be applied to optimise a design of pulp and paper process lines and to reduce of the associated costs.

Although the pulp and paper manufacturing are fundamentally the same, the final product can be quite different and directed for specific applications. The complex interactions between different pulp and paper components contribute to the distinct behavior from the other solid-liquid systems even if they are considered solid-liquid systems [6]. Understanding the pulp and paper manufacturing process requires knowledge in the chemistry, physics and fluid mechanics fields [7]. The fluid mechanics of the papermaking process includes: (*i*) the modelling of fiber suspensions, (*ii*) experimental methods to obtain the data necessary for validation and tuning the models, and (*iii*) the knowledge concerning the coupling between rheology and suspension characteristics [7]. As input, each stage needs the output information from the other stages which represents important challenges to get all the numerical and experimental information required.

The pulp flow starts when the shear stress is higher than the yield stress, $\tau_y$ [8] – see Figure 1. The suspension can present a fluid-like behavior when the shear stress exceeded $\tau_d$, also called fluidization point, and the network structure can be absolutely disrupted [8]. In this point, the fully developed turbulent flow starts and the pulps' hydrodynamic properties are analogous to those of water.

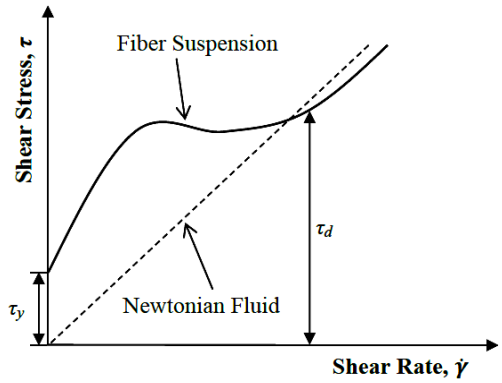


**Figure 1**: Stress-rate curve for a fiber suspension (adopted from [9]).

The existing studies report distinctive flow regimes and pressure loss curves from those of normal slurry or liquid flow systems – see Figure 2. The main flow regimes reported in

literature are the plug, transition and turbulent flow regimes, but there are also reported sub-regimes for each regime with well-defined shear mechanisms [6,9,10]. Initially, a plug of fibers is in contact with the pipe wall, an increased shear force distorts the plug and the motion begins when the yield stress has been surpassed. At low velocities, the pressure drop has larger values than those of water due to the flow of the suspension as a plug of fibers. $V_m$ (see Fig. 2) corresponds to the velocity where the maximum of the head loss curve at the plug flow occurs. The transition flow regime starts at velocity $V_m$. In this regime and intermediate velocities a central and intact plug is surrounded by a turbulent fiber-water annulus. The suspension components are in complex turbulent motion and the pressure drop is lower than the expected when the velocity is high [6]. $V_W$ is the velocity corresponding to the onset of drag reduction [6]. When the velocity is escalated beyond the point where the fiber suspension and water flow curves cross and become parallel, $V_W$, the whole suspension then becomes turbulent like a turbulent liquid and all velocities and consistency gradients disappear. The maximum of the drag reduction is represented by $V_{red}$.

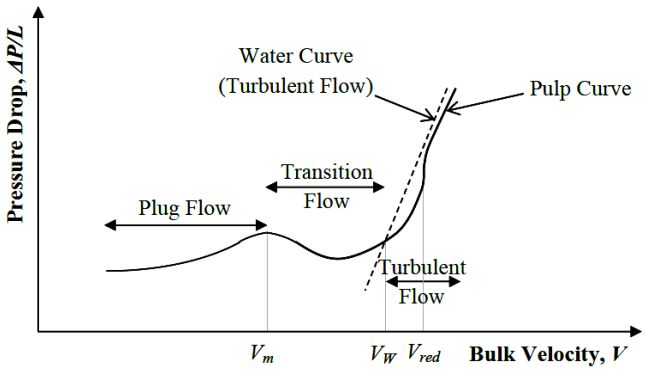


**Figure 2**: Pressure drop curve for pulp suspensions (adopted from [7,11]).

In the recent years, the interest on the numerical studies on the fiber suspension flows has been increasing and different mathematical models have been tested to describe this kind of flows. Two strategies are described in literature, the pseudo-homogeneous models and the multiphase models, each having a different complexity level and a specific domain of application. The multiphase models are suitable for dilute systems only due to their high level of complexity leading to huge computational efforts. The pseudo-homogenous models are appropriate for concentrated systems, where fiber-fiber and fiber-fluid interactions are represented by rheological pulp properties. From the authors' knowledge, the application of this kind of turbulence models to study the flow of turbulent pulp suspensions has not been undertaken so far. In literature, only a few studies are dedicated to concentrated pulp suspensions flows, but applying a different strategy. The application of low Reynolds $k$-$\varepsilon$ turbulence models (LRN) to study the polymers flow has been more studied than the application of such models to the fully developed turbulent flow of concentrated pulp suspensions.

The present work aims at numerical investigations of the fully developed turbulent pipe flow of concentrated *Eucalyptus* fiber pulp with CFD tools. The CFD model considering the Newtonian homogeneous one-phase fluid was reformulated to take into account the presence

of fibers in the flow. The strategy followed was a pseudo-homogeneous approach which is appropriate for high concentrated fiber suspensions. In this study, the CHC LRN turbulence model [1,2] was analyzed and modified in a proper way to reproduce the experimental data reported in literature regarding the turbulent pulp flow. As the reference the available experimental literature data of the pressure drop were used for the validation of the numerical results.

## 2 THE CHC LOW REYNOLDS TURBULENCE MODEL

Chang et al. [1,2] proposed a modified LRN $k$-$\varepsilon$ turbulence model to eliminate some difficulties of previous models to deal with a singularity occurring near the reattachment points of the recirculating flows in a sudden-expansion pipe. This new model indicates the proper near-wall limiting behavior and the singular defect occurring near the reattachment point when applied to separated flow is eliminated [2]. This model was applied to study wall heat transfer problems in flow with pipe expansion geometry and to test fully developed pipe flows. This model was able to reproduce the experimental data with a good agreement [1,2].

The present study addresses an incompressible, steady state, isothermal flow, without mass transfer, non-Newtonian fluid flow and 2D axisymmetrical flow. The complete system of governing equations is [1,2]:

$$\frac{1}{r}\left[\frac{\partial}{\partial x}\left(r\rho u\phi\right)+\frac{\partial}{\partial r}\left(r\rho v\phi\right)\right]=\frac{1}{r}\left[\frac{\partial}{\partial x}\left(r\Gamma_{\phi}\frac{\partial\phi}{\partial x}\right)+\frac{\partial}{\partial r}\left(r\Gamma_{\phi}\frac{\partial\phi}{\partial r}\right)\right]+S_{\phi} \tag{1}$$

where $x$ is the axial coordinate, $r$ is the radial coordinate, $\rho$ is the fluid density. The terms $S_{\phi}$, $\Gamma_{\phi}$ and $\phi$ are summarized in Table 1. . The model constants and wall boundary conditions of turbulent quantities are given in Table 2, while the damping functions of CHC model are presented in Table 3.

As shown by numerous experiments the presence of fibers leads to reduction of turbulence intensity as a consequence of inhibiting turbulent momentum transfer [12]. It means that for the fiber suspension flows the governing equations should be modified, in particular those describing the turbulent kinetic energy and turbulent dissipation rate. The application of LRN turbulence models to simulate the turbulent flow of polymers and particles is widely reported in literature, but it is poor and incomplete for pulp suspension flows. The strategy applied in this work was to consider the CHC turbulence model combined with the damping function $f_{\mu}$ adopted from [4], the model termed as CHC-Malin I. A series of simulation tests were performed considering the CHC-Malin II turbulence model to study the influence of the parameters values of the Malin's damping function on the numerical results, namely, on the pressure drop and dimensionless velocity profile.

## 3 NUMERICAL IMPLEMENTATION

All the cases tested were implemented in ANSYS FLUENT® CFD software package [ANSYS FLUENT® 13.0.0, ANSYS FLUENT Inc., 2010] using User-Defined Functions (UDF), i.e. the own developed procedures linked to the source code. The CHC turbulence model implemented using UDF is capable to reproduce precisely the numerical results obtained with the in-built CHC turbulence model [3].

**Table 1**: The structure of terms $S_\phi$, $\Gamma_\phi$ and $\phi$ in the general transport equation (1) [1,2].

| *equation* | $\phi$ | $\Gamma_\phi$ | $S_\phi$ |
|---|---|---|---|
| *continuity* | 1 | 0 | 0 |
| *momentum axial* | *u* | $\mu_{eff} = \mu + \mu_t$ | $-\frac{\partial P}{\partial x} + \frac{\partial}{\partial x}\left(\mu_{eff}\frac{\partial u}{\partial x}\right) + \frac{1}{r}\frac{\partial}{\partial r}\left(r\mu_{eff}\frac{\partial v}{\partial x}\right)$ |
| *momentum radial* | *v* | $\mu_{eff} = \mu + \mu_t$ | $-\frac{\partial P}{\partial r} + \frac{\partial}{\partial r}\left(\mu_{eff}\frac{\partial u}{\partial r}\right) + \frac{1}{r}\frac{\partial}{\partial r}\left(r\mu_{eff}\frac{\partial v}{\partial r}\right) - 2\mu_{eff}\frac{v}{r^2}$ |
| *t.k.e.* | *k* | $\mu + \mu_t / \sigma_k$ | $G_k - \rho\varepsilon$ |
| *t.d.r.* | $\varepsilon$ | $\mu + \mu_t / \sigma_\varepsilon$ | $\left(C_{\varepsilon 1} f_1 G_k - C_{\varepsilon 2} f_2 \rho\varepsilon\right)\cdot \varepsilon / k$ |

$$G_k = \mu_t\left\{2\left[\left(\frac{\partial u}{\partial x}\right)^2 + \left(\frac{\partial v}{\partial r}\right)^2 + \left(\frac{v}{r}\right)^2\right] + \left(\frac{\partial v}{\partial x} + \frac{\partial u}{\partial r}\right)^2\right\};\ \mu_t = \rho C_\mu f_\mu \frac{k^2}{\varepsilon}$$

**Table 2**: Model constants and wall boundary conditions (BC) in CHC turbulence model [1,2].

| Model | $C_\mu$ | $C_{\varepsilon 1}$ | $C_{\varepsilon 2}$ | $\sigma_\varepsilon$ | $\sigma_k$ | $\varepsilon_w - B.C.$ | $k_w - B.C.$ |
|---|---|---|---|---|---|---|---|
| CHC | 0.09 | 1.44 | 1.92 | 1.0 | 1.3 | $\upsilon\left(\partial^2 k / \partial y^2\right)$ | 0 |

**Table 3**: Damping functions of CHC turbulence model [1,2].

| Model | $f_\mu$ | $f_2$ |
|---|---|---|
| CHC [(1)] | $\left[1 - exp\left(-0.0215 Re_k\right)\right]^2 \times \left(1 + 31.66 / Re_t^{5/4}\right)$ | $\left[1 - 0.01 exp\left(-Re_t^2\right)\right] \times \left[1 - exp\left(-0.0631 Re_k\right)\right]$ |
| CHC-Malin I [(2)] | $\left[1 - exp\left(-0.0165 Re_k / n^{1/4}\right)\right]^2 \times \left(1 + 20.5/Re_t\right)$ | $\left[1 - 0.01 exp\left(-Re_t^2\right)\right] \times \left[1 - exp\left(-0.0631 Re_k\right)\right]$ |
| CHC-Malin II [(3)] | $\left[1 - exp\left(-A \cdot Re_k / n^C\right)\right]^2 \times \left(1 + B/Re_t\right)$ | $\left[1 - 0.01 exp\left(-Re_t^2\right)\right] \times \left[1 - exp\left(-0.0631 Re_k\right)\right]$ |

[(1)] CHC LRN turbulence model; [(2)] CHC LRN turbulence model considering the damping function $f_\mu$ of Malin [4]; [(3)] CHC LRN turbulence model considering the damping function $f_\mu$ of Malin [4], but with modified model parameters.

$$f_1 = 1.0;\ Re_t = \frac{k^2}{\varepsilon\upsilon};\ Re_k = \frac{y k^{1/2}}{\upsilon}$$

Turbulent kinetic energy and its dissipation rate are introduced as scalar quantities. In the CFD solver, the built-in turbulence equations are turned off. User Defined Scalar (UDS) Sources are used to add the source terms in the turbulence (scalar) equations and the diffusivities are introduced as User Defined Scalar Diffusivity in the material properties. Turbulent viscosity given in Table 1 is introduced as Turbulent Viscosity in the model.

In Ansys Fluent solver, the partial differential equations are discretized using the finite volume method [13]. The complete set of equations represented by general equation (1) is integrated for each individual control volume resulting on algebraic equations for the unknown discrete dependent variables. The algebraic equations can then be solved numerically with a control-volume-based technique. The linearization of the discretized equations results in a linear system of equations and its solution yield updated values for the dependent variables. The first-order upwind scheme is chosen to discretized spatially the differential conservation equations, i.e. it is assumed that the quantities of the variables at cell faces are similar to the value in the cell centre that represents a cell-average value [13]. The Simple algorithm was chosen in which the mass conservation is implemented by reformulating the continuity equation which derives an additional condition for the pressure using a correlation between velocity and pressure corrections and, in this way, obtain the pressure field [13]. All cases studied include the fully developed turbulent pipe flow (Table 4). The numerical solution of the complete system of equations involves boundary conditions related with the inlet and outlet flow, with the wall and pipe axis. The inlet and outlet are linked as periodic boundary conditions and there is imposed the mass flow rate at the inlet. The pipe axis was considered as axis boundary condition. For each UDS (User Defined Scalar), the boundary conditions at the wall are given in Table 2. The numerical domain (Figure 3) was discretized with a structured non-uniform (refined in the near-wall region) mesh with the characteristics given in Table 4. The convergence criterion was the residuals and the solution was considered converged when they had met a specified convergence level ($1\times10^{-5}$).

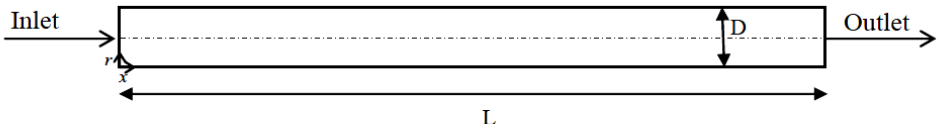


**Figure 3**: Model geometry considered [14].

**Table 4**: Numerical mesh characterisation.

| *L [m]* | *D [m]* | *Mesh nodes number* [4] | *R*[5] |
|---|---|---|---|
| 1.0 | 0.07620 | 20×118 | 1.05 |

[4] Number of nodes according to *x* and *r* coordinates, respectively. [5] Interval length ratio.

## 4 TEST CASES

The numerical tests were performed to reproduce the experimental flow data of a turbulent flow of *Eucalyptus* pulp (fiber average length of 0.706 mm [15]) for different experimental flow conditions (flow rate and consistency). The experimental information on the viscosity of the pulp suspensions was applied to obtained correlations to be introduced into the CFD code and the head loss in the pipe was used to validate the mathematical model.

The pulps' rheological characterization didn't have yet a standard procedure or equipment to obtain the rheological data. Modified rotational rheometers, conventional rheometers, pipe rheometers, NMRI techniques and UVP-PD techniques (off-line and in-line techniques) can be applied to obtain the material pulp properties. The rheological data required in the present work were obtained using an off-line technique, an adapted Searle-type rotational rheometer –

plate viscometer [8,16]. Two *Eucalyptus* pulp consistencies equal to 1.50 and 2.50 % (w/w) were considered in the present study. The rheogram and apparent viscosity representation for the pulp with consistency equal to 1.50 % (w/w) can be in [14]. The apparent viscosity was obtained considering the viscosity of a Newtonian fluid with the same resistance to the flow as the pulp and can be given by the following equation [14]:

$$\mu_{app} = K\left(\dot{\gamma}\right)^{n-1} \tag{2}$$

where $\mu_{app}$ is the apparent viscosity, $K$ is the consistency index and $n$ is the flow behavior index (Table 3). The flow data under interest (Table 5) were adopted from [6,15] including the experimental results obtained in a pilot rig properly adapted to study the flow of pulp suspensions.

**Table 5**: Flow cases studied [3,6,14,15].

| $c$ [% w/w] | $K$ | $n$ | $U_b$ [6] [m·s$^{-1}$] | $F_b$ [kg·s$^{-1}$] | $Re_w$ [7] | $\Delta P/L_{water}$ [8] [Pa·m$^{-1}$] | $\Delta P/L_{exp.}$ [9] [Pa·m$^{-1}$] | *Case* | $\Delta P/L_{num.}$ [10] [Pa·m$^{-1}$] |
|---|---|---|---|---|---|---|---|---|---|
| 1.50 | 0.28 | 0.53 | 4.49 | 20.4 | 340500 | 1885.16 | 829.1 | *A0* | 360.19 |
| 1.50 | 0.28 | 0.53 | 6.21 | 28.3 | 470900 | 3419.65 | 1288.69 | *B0* | 3355.60 |
| 2.50 | 10.72 | 0.25 | 4.90 | 20.3 | 371600 | 2212.55 | 1578.94 | *C0* | 2157.18 |
| 2.50 | 10.72 | 0.25 | 5.55 | 25.3 | 402900 | 2781.05 | 1753.79 | *D0* | 2335.43 |

[6] Mean inlet pulp velocity. [7] Reynolds number calculated based on the wall viscosity [17]. [8] Only flow of water in the same pipe. [9] Experimental pressure drop value for pulp flow. [10] Numerical pressure drop value for pulp flow.

## 5 RESULTS AND DISCUSSION

### 5.1 CHC turbulence model

The UDF implementing the CHC LRN turbulence model was validated by the authors in the previous work [3]. The validation was made by comparing the results produced with the use of the UDF with those obtained from the built-in Ansys Fluent model. An excellent agreement was found between both the own-developed and built-in model results.

Despite of a *drag reduction* reproduced with the use of the CHC turbulence model for all cases, it is evident that the numerical pressure drops are still not acceptable for the pulp flow cases tested (Table 5).

The main results evaluated in the present work are the behavior of the dynamic viscosity, dimensionless velocity, turbulent kinetic energy and its dissipation rate, according to $r$, since they are the main variables modified in relation to the Newtonian one-phase turbulence model.

In Table 6 the main results obtained with the CHC turbulence model are summarized. For the pulp suspensions flow it is expected that a peculiar S-shaped profile near the wall was obtained for the dimensionless velocity as a function of dimensionless distance to the pipe wall [5]. A better agreement between the numerical pressure drops and the experimental ones was achieved in the cases where the dimensionless velocity profile follows the tendency

reported in [5]. The dynamic velocity profiles represent the higher flow resistance in the pipe center where the number of fibers is higher. For the lower consistency cases, the dynamic viscosity profile is more uniform in the radial direction due to the lower number of fibers in the flow and the viscosity is very similar across most of the pipe sectional area. All the viscosity profiles reflect the higher resistance to the flow in the central region of the pipe where the fibers are more concentrated forming the core region. Regarding the dimensionless velocity profiles, the abrupt transition in viscosity from the core region to the water annulus for c=2.50% (w/w) is not as smooth as in the cases where c=1.50% (w/w). This fact is due to the higher concentration/fiber number in the core region when c=2.50% (w/w) and, also, because the transition in the dynamic viscosity is more abrupt in those cases. The peculiar S-shaped profile is more evident for c=1.50% (w/w) and $Re_w$=340500 which can be due to the *k* values near the wall are being correctly described by the damping functions which is also observed by the reduction of $\varepsilon$ near the wall.

**Table 6**: Numerical results – CHC model.

*Dynamic viscosity*

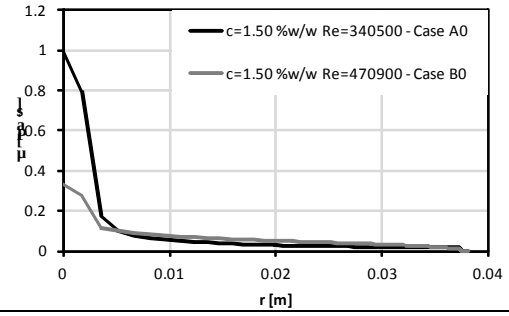


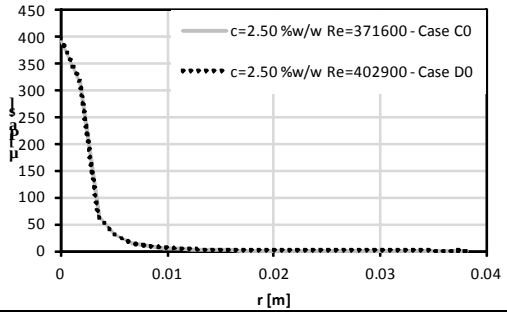


*Dimensionless velocity*

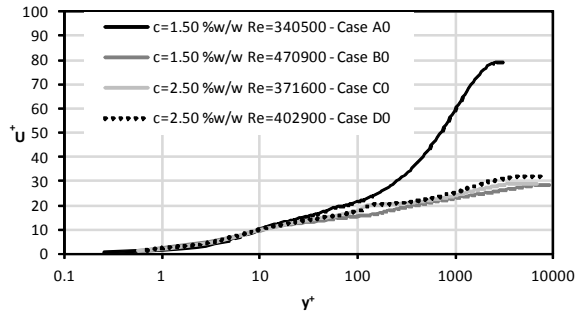


*Turbulent kinetic energy*

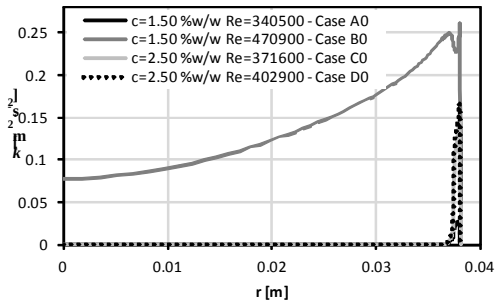


*Dissipation rate of k*

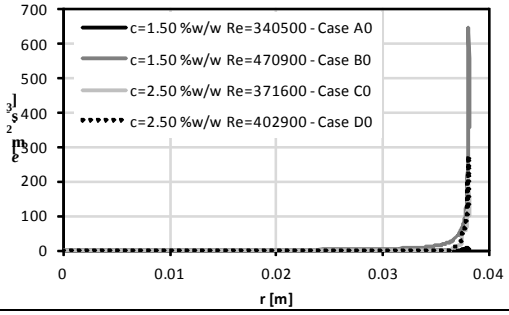

## 5.2 Modified CHC turbulence model

The application of the CHC turbulence model to the pulp flow leads to lower pressure drop than that when considering the water flow in the same pipe. However, the pressure drop values are higher than the experimental ones for the *Eucalyptus* pulp flow. The modification of the damping function, $f_\mu$, according to [4] was tested. This kind of damping function was applied successfully to predict the flow of power-law fluids. The influence of three parameters on the damping function and on the main numerical results was investigated. A series of test cases performed is indicated in Table 7. The numerical pressure drop values and model parameters tested are presented in Table 8.

The modification on the damping function, $f_\mu$, according to [4] had no a strong impact on the numerical pressure drop which means that the values proposed for the power-law fluid flow cases are not appropriate for the *Eucalyptus* pulp flow cases tested. In general, this modification leads to closer pressure drop values to those obtained with the CHC turbulence model without modification. The most sensitive case to the modification on the parameters is the pulp with c=1.50% (w/w) and $U_b$=4.49 $m \cdot s^{-1}$ which can be explained by the fact that this case is very close to the transition regime and the turbulent flow most likely is not fully developed. The numerical pressure drop is strongly sensitive to the parameter *C* and a good correlation between the experimental and numerical pressure drop values can be achieved by modifying this term. A proposal for an optimal value of *C* is presented in Table 9 and its values depend on the cases tested which suggest that the parameter *C* can be related with the flow and pulp characteristics. This kind of dependence of *C* on the flow and pulp characteristics will be analyzed in a future work.

**Table 7**: Flow cases tested (see Table 6).

| *Case* | *1* | *2* | *3* | *4* | *5* | *6* | *7* | *8* | *9* |
|---|---|---|---|---|---|---|---|---|---|
| *Model* | CHC-Malin I | CHC-Malin II | | | | | | | |
| *A* | 0.0165 | 0.0125 | 0.0195 | 0.0165 | 0.0165 | 0.0165 | 0.0165 | 0.0165 | 0.0165 |
| *B* | 20.5 | 20.5 | 20.5 | 10.25 | 30.75 | 20.5 | 20.5 | 20.5 | 20.5 |
| *C* | 0.25 | 0.25 | 0.25 | 0.25 | 0.25 | 1.125 | 1.05 | 2.00 | 1.975 |

**Table 8**: Numerical pressure drop values – CHC Malin II.

| *Case* | *c* [% w/w] | $U_b$ (6) [$m \cdot s^{-1}$] | $F_b$ [$kg \cdot s^{-1}$] | $Re_w$ (7) | $\Delta P/L_{exp.}$ (9) [$Pa \cdot m^{-1}$] | $\Delta P/L_{num.}$ (10) [$Pa \cdot m^{-1}$] | $\varepsilon$ (11) [%] |
|---|---|---|---|---|---|---|---|
| *A1* | 1.50 | 4.49 | 20.4 | 340501 | 829.1 | 360.53 | 56.5 |
| *B1* | 1.50 | 6.21 | 28.3 | 470937 | 1288.69 | 3331.68 | 158.5 |
| *C1* | 2.50 | 4.90 | 20.3 | 371593 | 1578.94 | 2152.18 | 36.3 |
| *D1* | 2.50 | 5.55 | 25.3 | 402886 | 1753.79 | 2333.18 | 33.0 |
| *A2* | 1.50 | 4.49 | 20.4 | 340501 | 829.1 | 1667.80 | 101.2 |
| *B2* | 1.50 | 6.21 | 28.3 | 470937 | 1288.69 | 3167.18 | 145.8 |
| *C2* | 2.50 | 4.90 | 20.3 | 371593 | 1578.94 | 2151.61 | 36.3 |
| *D2* | 2.50 | 5.55 | 25.3 | 402886 | 1753.79 | 2342.07 | 33.5 |
| *A3* | 1.50 | 4.49 | 20.4 | 340501 | 829.1 | 359.36 | 56.7 |

| | | | | | | | |
|---|---|---|---|---|---|---|---|
| *B3* | 1.50 | 6.21 | 28.3 | 470937 | 1288.69 | 3381.53 | 162.4 |
| *C3* | 2.50 | 4.90 | 20.3 | 371593 | 1578.94 | 2139.57 | 35.5 |
| *D3* | 2.50 | 5.55 | 25.3 | 402886 | 1753.79 | 2319.58 | 32.3 |
| *A4* | 1.50 | 4.49 | 20.4 | 340501 | 829.1 | 361.30 | 56.4 |
| *B4* | 1.50 | 6.21 | 28.3 | 470937 | 1288.69 | 3343.25 | 159.4 |
| *C4* | 2.50 | 4.90 | 20.3 | 371593 | 1578.94 | 2163.30 | 37.0 |
| *D4* | 2.50 | 5.55 | 25.3 | 402886 | 1753.79 | 2342.07 | 33.5 |
| *A5* | 1.50 | 4.49 | 20.4 | 340501 | 829.1 | 359.46 | 56.6 |
| *B5* | 1.50 | 6.21 | 28.3 | 470937 | 1288.69 | 3317.22 | 157.4 |
| *C5* | 2.50 | 4.90 | 20.3 | 371593 | 1578.94 | 2139.93 | 35.5 |
| *D5* | 2.50 | 5.55 | 25.3 | 402886 | 1753.79 | 2320.96 | 32.3 |
| *A6* | 1.50 | 4.49 | 20.4 | 340501 | 829.1 | 317.22 | 61.7 |
| *B7* | 1.50 | 6.21 | 28.3 | 470937 | 1288.69 | 418.98 | 67.5 |
| *C8* | 2.50 | 4.90 | 20.3 | 371593 | 1578.94 | 1581.67 | 0.2 |
| *D9* | 2.50 | 5.55 | 25.3 | 402886 | 1753.79 | 1774.19 | 1.2 |

(6) Mean inlet pulp velocity. (7) Reynolds number calculated based on the wall viscosity [17]. (9) Experimental pressure drop value for pulp flow. (10) Numerical pressure drop value for pulp flow. (11) Relative error between the experimental and numerical pressure drop ($|\Delta P/L_{exp.}-\Delta P/L_{num.}|/\Delta P/L_{exp.}$).

The modification of the damping function affects the velocity profile, turbulent kinetic energy and its dissipation. The behavior of these variables is important to be analyzed since the *drag reduction* effect is reflected by the decay of turbulence and by an S-shaped dimensionless velocity profile. In Table 9 the profiles of $u^+$, $k$ and $\varepsilon$ are presented for the cases where the numerical pressure drops are closer to the experimental ones – Cases *A6*, *B7*, *C8* and *D9*. For the lower consistency cases, the pressure drop is lower than the experimental values which means that the modifications of the damping function lead to excessive reduction of the turbulence intensity. As can be observed, for the higher consistency cases the dimensionless velocity profile reflects the higher number of fibers in the core region which creates a higher resistance to the flow and a more uniform radial velocity distribution. The peculiar S-shaped profile is more evident for the cases of c=1.50% (w/w) and the three regions described in [5] can be identified – the near wall, yield and core regions. At the turbulence level, the higher number of fibers (c=2.50% (w/w)) is reflected in the attenuation of turbulence. The increase of $C$ in relation to the CHC turbulence model leads to an increase of the damping function and in this way to the reduction of turbulent kinetic energy. The most sensitive case to the $C$ value is c=2.50% (w/w) and $U_b$=4.90 $m \cdot s^{-1}$ which corresponds to the highest Reynolds number based on the wall viscosity and lower dynamic viscosity.

## 6 CONCLUSIONS

In the current study a numerical work concerning the *Eucalyptus* pulp flow using the commercial software Ansys Fluent is presented. The LRN CHC turbulence model was reproduced using User-Defined-Function. The non-Newtonian behavior of the pulp was introduced by considering the local viscosity of the pulp as a function of local shear rate. Moreover, a water annulus near the wall surrounding the core region was taken into account.

**Table 9**: Numerical results – modified CHC model.

*Dimensionless velocity*

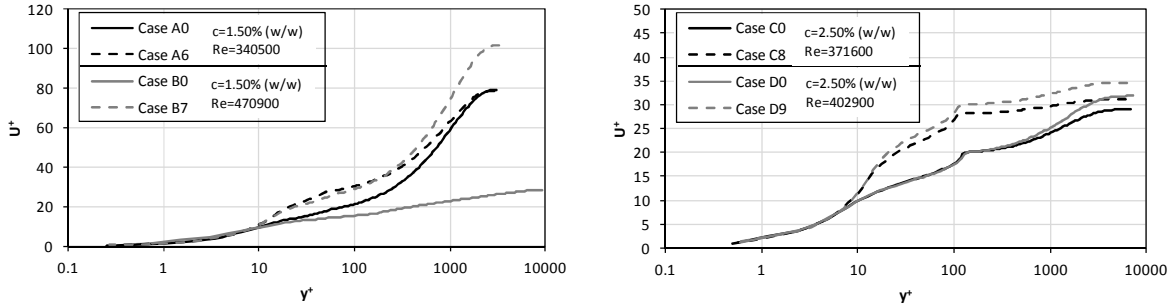


*Turbulent kinetic energy*

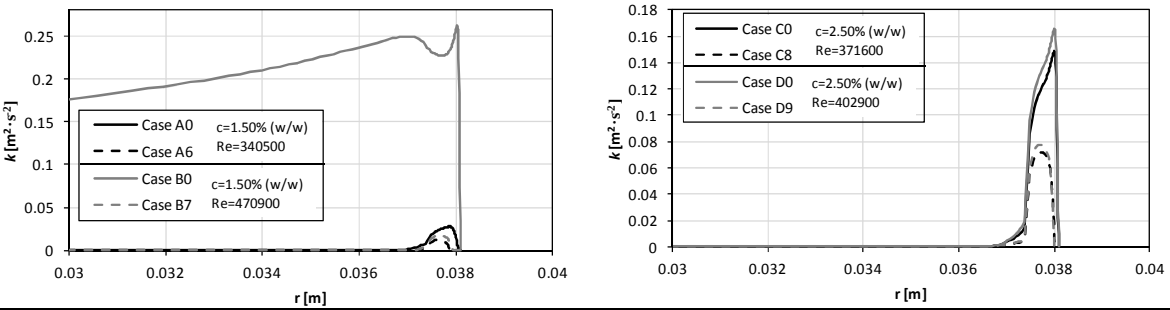


*Dissipation rate of k*

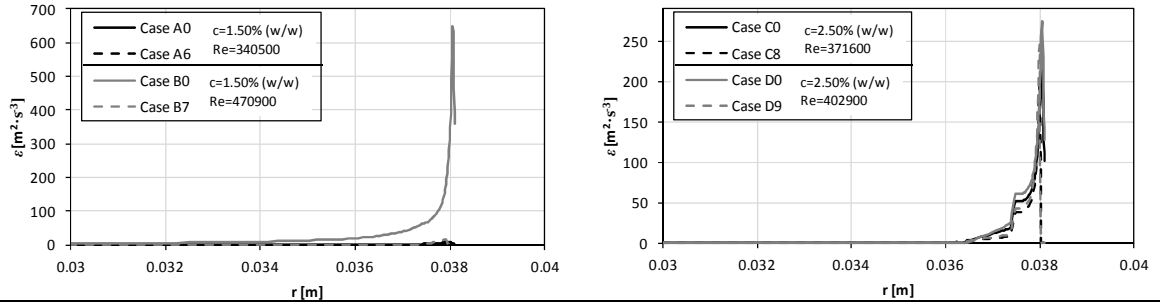


The original LRN CHC turbulence model was modified taking into account the modifications presented in [4] for the power-law fluid flow.

The main conclusions are:

- The application of the LRN CHC turbulence model [1,2] and also the introduction of the non-Newtonian behavior of the pulp is able to reproduce the *drag reduction* effect observed experimentally for the pulp flow.
- The application of the modified damping function, $f_\mu$, according to [4] was not able to improve the numerical results in satisfactory way.
- The numerical results can be improved considerably by modifying the $C$ term of damping function, $f_\mu$, (Tables 3, 8 and 9).
- The modification on the parameter $C$ in the CHC-Malin II presented in this work was optimized for the higher consistency cases.
- For the lower consistency cases the damping function CHC-Malin II turbulence model reduces considerably the turbulence and the pressure drop is lower than the

experimental one.

- In a future work an expression for the parameter *C* related with the flow and pulp characteristics will be studied.

## ACKNOWLEDGMENTS

The present work was developed under the project PTDC/QUE-QUE/112388/2009, financed by FCT/MCTES(PIDDAC) and co-financed by the EU Regional Development Fund (ERDF) through the program COMPETE (POFC) and in relation with COST Action FP1005.

## REFERENCES

[1] Chang, K.C.; Hsieh, W.D. and Chen, C.S. A modified low-Reynolds-number turbulence model applicable to recirculating flow in pipe expansion. *J. of Fluids Engineering* (1995) **117**:417-423.

[2] Hsieh, W.D. and Chang, K.C. Calculation of wall heat transfer in pipe-expansion turbulent flows. *International Journal of Heat and Mass Transfer* (1996) **18**:3813-3822.

[3] Cotas, C.; Silva, R.; Garcia, F.; Ferreira, P.; Faia, P.; Asendrych, D. and Rasteiro, M.G. Application of different low-Reynolds *k-ε* turbulence models to model the flow of concentrated pulp suspensions in pipes. Proceedings of The 7th World Congress on Particle Technology (WCPT 7), 19-22 May 2014, Beijing, China.

[4] Malin, M.R. Turbulent pipe flow of power-law fluids, *International Communications in Heat and Mass Transfer* (1997) **24**:977-988.

[5] Jäsberg, A. *Flow behavior of fibre suspensions in straight pipes: new experimental techniques and multiphase modeling*. PhD thesis, University Jyväskylä, Finland (2007).

[6] Ventura, C.; Garcia, F.; Ferreira, P. and Rasteiro, M. Flow dynamics of pulp fiber suspensions. *TAPPI Journal* (2008) **7**:20-26.

[7] Lundell, F.; Söderberg, L.D. and Alfredsson, P.H. Fluid mechanics of papermaking. *Annual Review of Fluid Mechanics* (2011) **43**:195-217.

[8] Ventura, C.; Blanco, A.; Negro, C.; Ferreira, P., Garciaa, F. and Rasteiro, M. Modeling pulp fiber suspension rheology. *TAPPI Journal* (2007) **6**:17-23.

[9] Gullichsen, J. and Härkönen, E. Medium consistency technology I. Fundamental data. *TAPPI Journal* (1981) **64**:69-72.

[10] Fock, H.; Wiklund, J. and Rasmuson, A. Ultrasound velocity profile (UVP) measurements of pulp suspension flow near the wall. *Journal of Pulp and Paper Science* (2009) **35**:26-33.

[11] TAPPI TIP 0410-15. *Optimum consistency for pumping pulp*, TAPPI (2001).

[12] Yang, W.; Shen, S. and Ku, X. A new model of turbulent fiber suspension and its application in the pipe flow. *The Canadian Journal of Chemical Engineering* (2013) **91**:992-999.

[13] ANSYS FLUENT Theory Guide, Ansys Fluent 14.0, (2011).

[14] Cotas, C.; Garcia, F.; Faia, P.; Ferreira, P.; Coimbra, A.; Fuente, E.; Asendrych, D. and Rasteiro, M.G. Numerical simulation of a turbulent fiber suspension flow in pipes using the CFD software Ansys Fluent. Proc. Congress on Numerical Methods in Engineering CMN2013, Jesus Mari Blanco, Irene Arias, Alberto Pena, Jose Miranda Guedes, Nuno Silvestre, Miguel Silva (Eds.), 25-28 June 2013, Bilbao, Spain, pp.546-565.

[15] Ventura, C.A.F.; Garcia, F.A.P.; Ferreira, P.J. and Rasteiro, M.G. Modeling the turbulent flow of pulp suspensions. *Industrial & Engineering Chemistry Research* (2011) **50**:9735:9742.

[16] Blanco, A.; Negro, C.; Fuente, E. and Tijero, J. Rotor selection for a Searle-type device to study the rheology of paper pulp suspensions. *Chemical Engineering and Processing* (2007) **46**:37-44.

[17] Rudman, M. and Blackburn, H.M. Direct numerical simulation of turbulent non-Newtonian flow using a spectral element method. *Applied Mathematical Modelling* (2006) **30**:1229-1248.